Triboelectric nanogenerator exhibiting ultrahigh charge density and energy density

Xiaoru Liu,[ab] Zhihao Zhao,*[abc] Yikui Gao,[ab] Yang Nan,[ab] Yuexiao Hu,[a] Ziting Guo,[ab] Wenyan Qiao,[ab] Jing Wang,[ab] Linglin Zhou,[abc] Zhong Lin Wang*[acde] and Jie Wang*[abc]

[a] *Beijing Institute of Nanoenergy and Nanosystems, Chinese Academy of Sciences, Beijing, 100083, P. R. China*

[b] *School of Nanoscience and Engineering, University of Chinese Academy of Sciences, Beijing, 100049, P. R. China*

[c] *Guangzhou Institute of Blue Energy, Knowledge City, Huangpu District, Guangzhou, 510555, P. R. China*

[d] *School of Materials Science and Engineering, Georgia Institute of Technology, Atlanta, GA 30332, USA*

[e] *Yonsei Frontier Lab, Yonsei University, Seoul, 03722, Republic of Korea*

*Corresponding Author: Z. Zhao: zhaozhihao@binn.cas.cn; Z. L. Wang: zhong.wang@mse.gatech.edu; J. Wang: wangjie@binn.cas.cn;
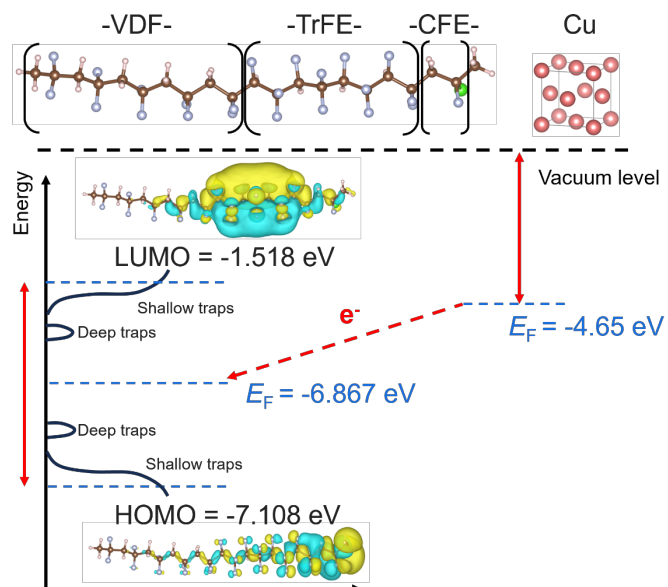
Table of Contents

Fig. S1 The electron density distribution of HOMO, LUMO, E_F and distribution of trap states on the energy band for P(VDF-TrFE-CFE).
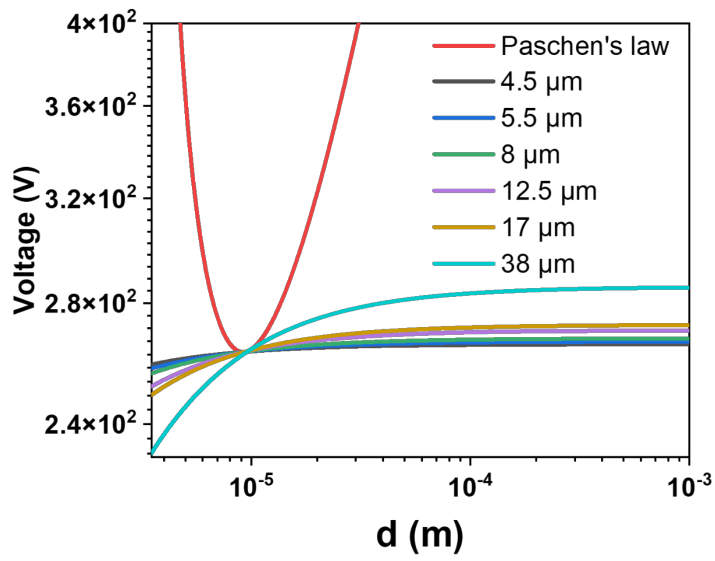
Fig. S2 Breakdown voltage and gap voltage across the triboelectric layers at various distances in TENG with different thickness' P(VDF-TrFE-CFE) films.

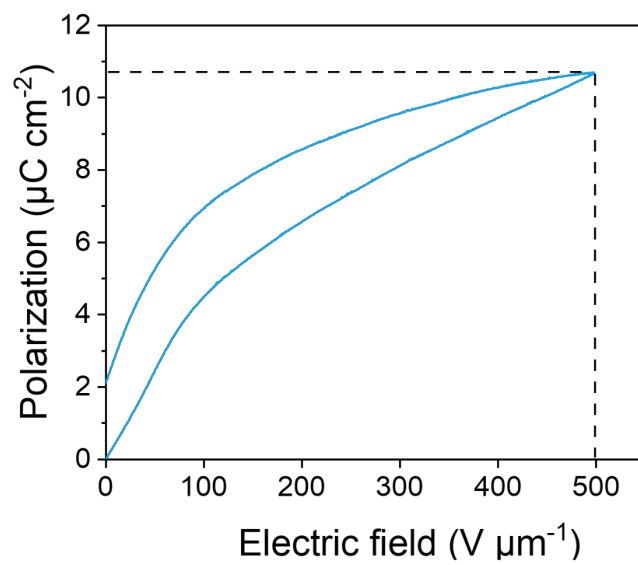**Fig. S3** The optical image of P(VDF-TrFE-CFE) film.

Fig. S4 The polarization loop of 8 μm P(VDF-TrFE-CFE) film at 500 V μm^{-1}.

Origin **Pressed**

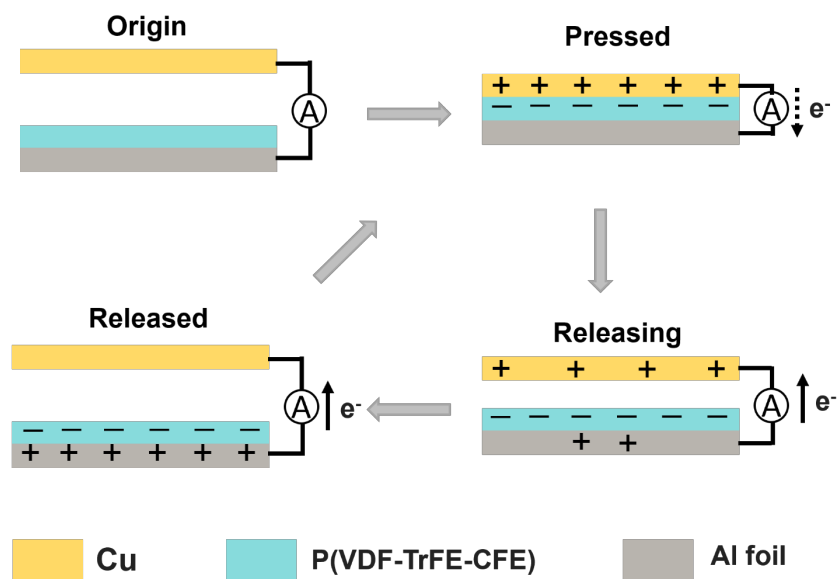**Released** **Releasing**

■ Cu ■ P(VDF-TrFE-CFE) ■ Al foil

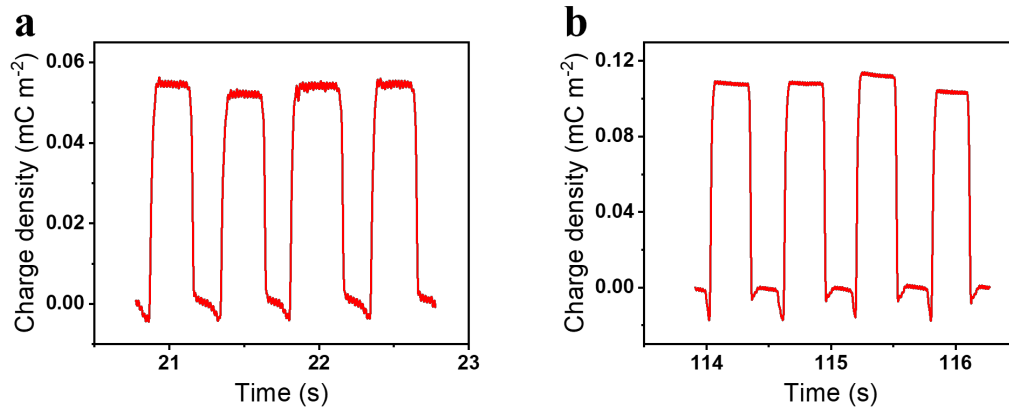**Fig. S5** Schematic diagram of measurement method in experiment with P(VDF-TrFE-CFE) films.

Fig. S6 The output performance of CS-TENG with 8 μm P(VDF-TrFE-CFE) film at 1.4 Hz. (a) Air condition. (b) Vacuum condition.
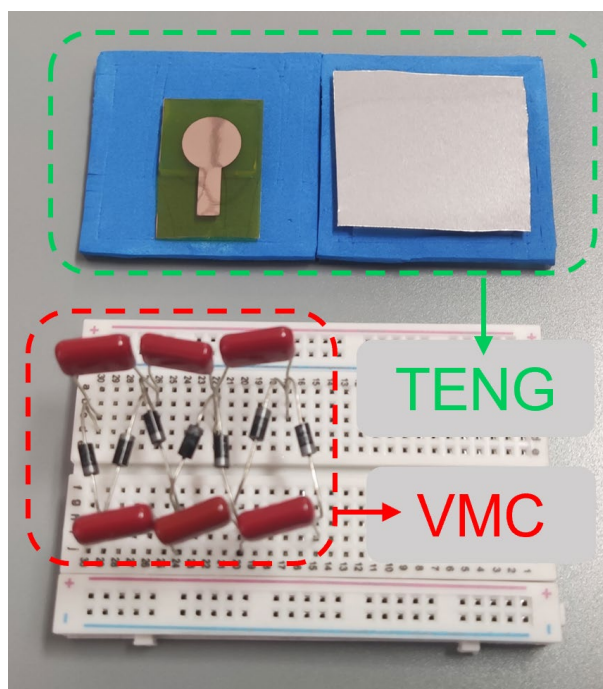
Fig. S7 Photograph of two parts of SCE-TENG.
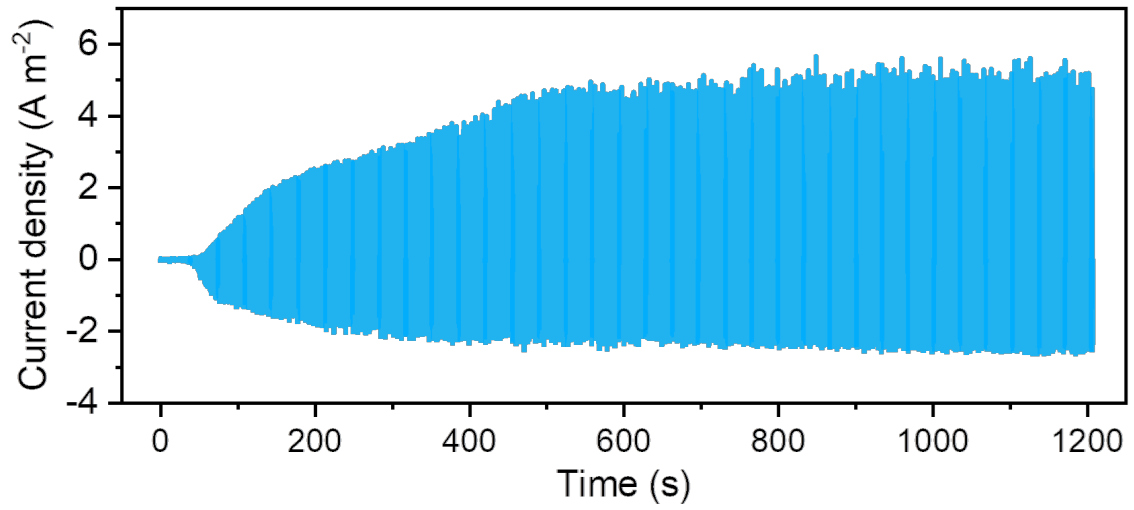
Fig. S8 Current accumulation process of SCE-TENG under 10 nF capacitor in circuit and N = 3 (f = 1.4 Hz).
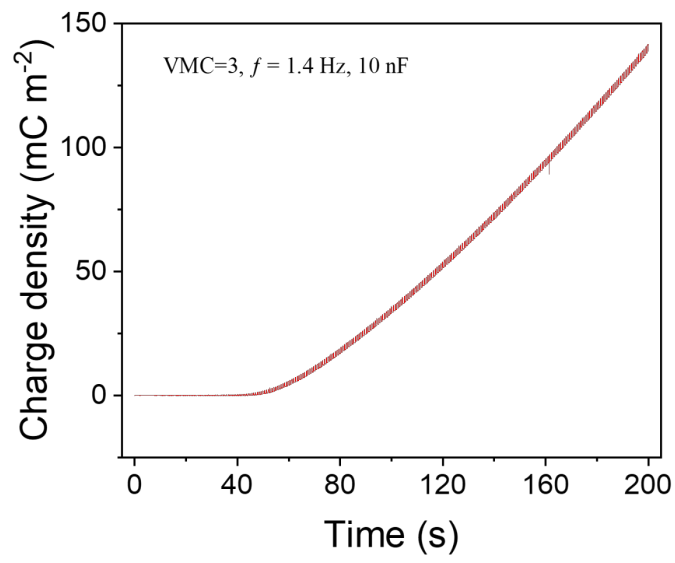
Fig. S9 The charge density accumulation process of SCE-TENG using 8 μm P(VDF-TrFE-CFE).
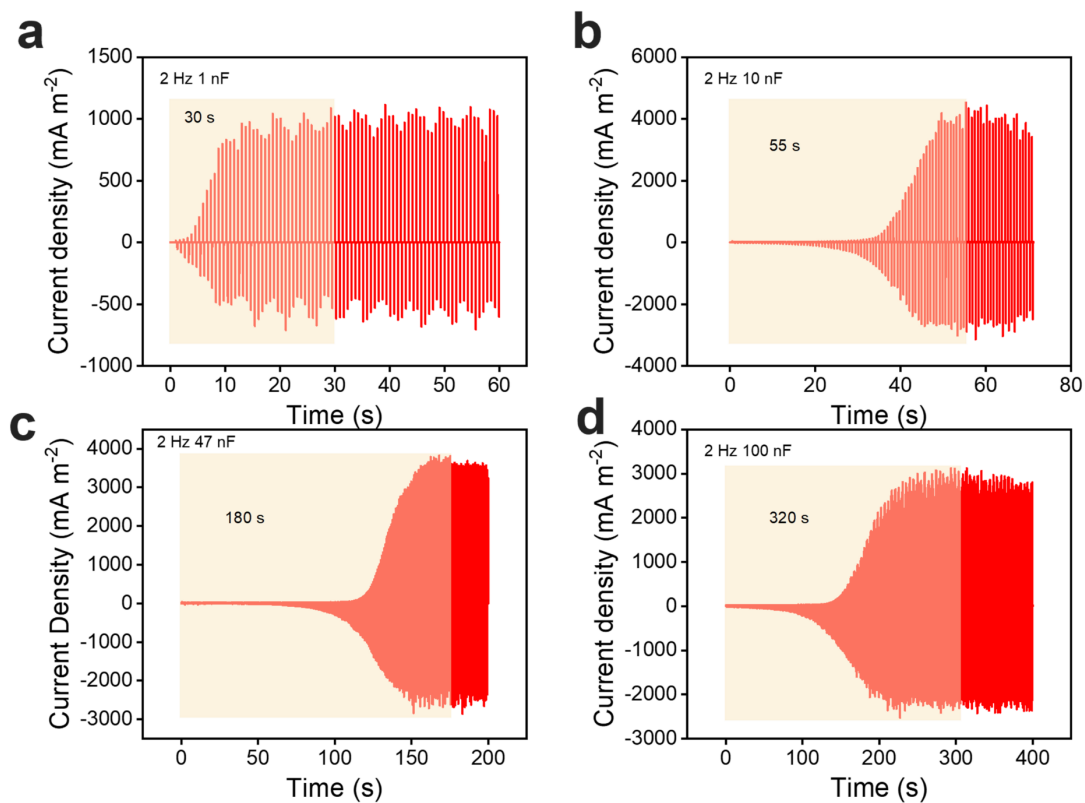
Fig. S10 The current density accumulation process of SCE-TENG using 8 μm P(VDF-TrFE-CFE) under different capacitor. (a) 1 nF. (b) 10 nF. (c) 47 nF. (d) 100 nF.
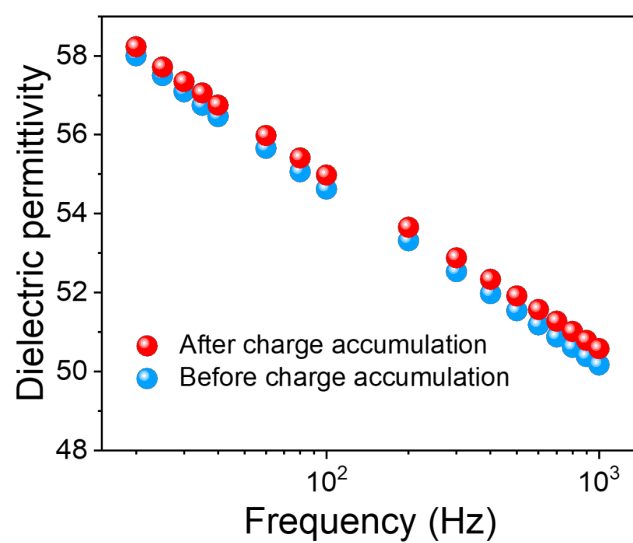
Fig. S11 Comparison of dielectric permittivity before and after charge accumulation for P(VDF-TrFE-CFE) film in a SCE-TENG.
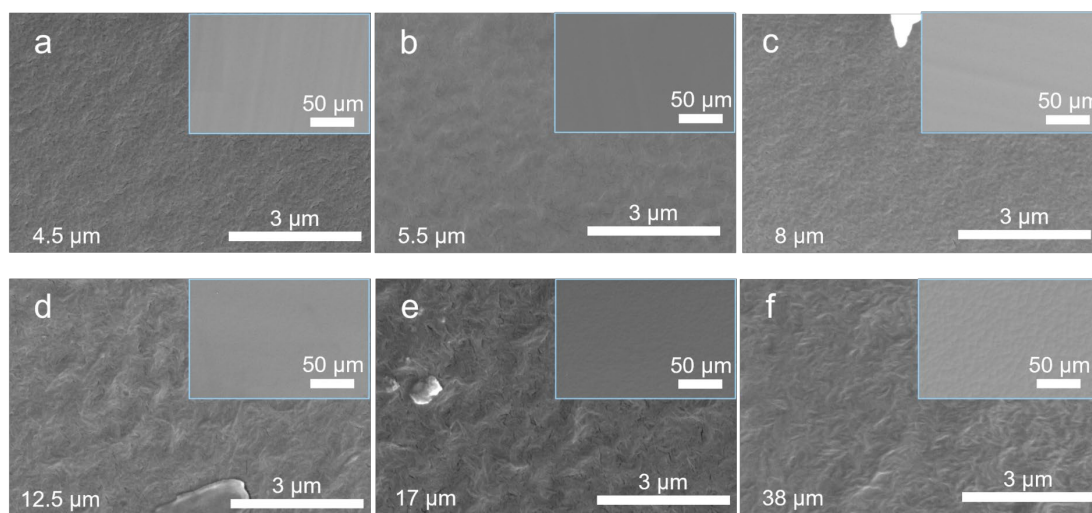
Fig. S12 Surface SEM images of P(VDF-TrFE-CFE) film with different thickness. (a) 4.5 µm. (b) 5.5 µm. (c) 8 µm. (d) 12.5 µm. (e) 17 µm. (f) 38 µm.
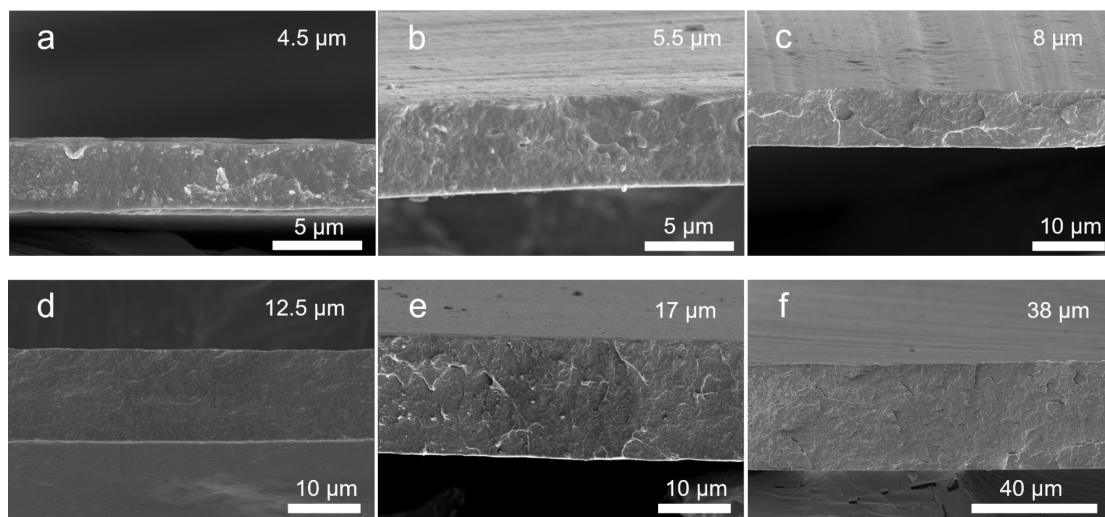
Fig. S13 Cross-sectional SEM images of P(VDF-TrFE-CFE) with different thickness. (a) 4.5 μm. (b) 5.5 μm. (c) 8 μm. (d) 12.5 μm. (e) 17 μm. (f) 38 μm.
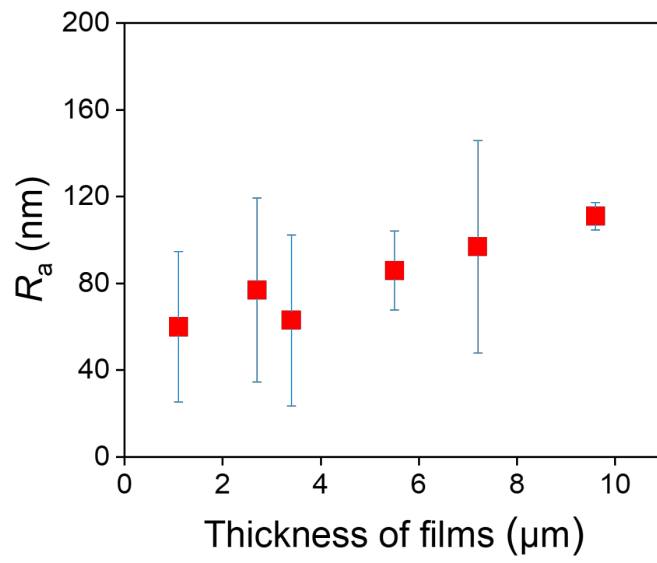
Fig. S14 The roughness of P(VDF-TrFE-CFE) with different thickness.
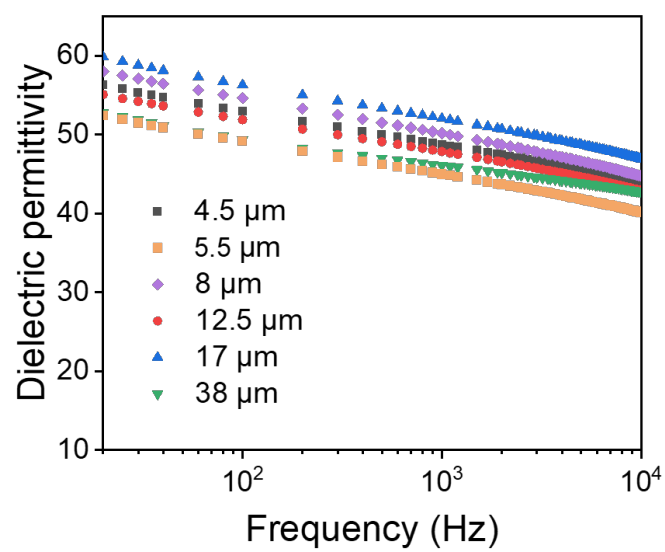
Fig. S15 Dielectric permittivity of P(VDF-TrFE-CFE) films with different thickness.
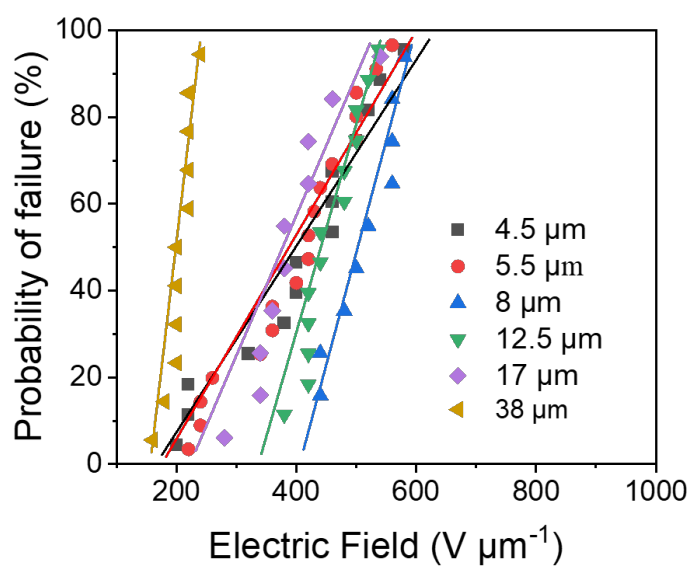
Fig. S16 Weibull distribution of P(VDF-TrFE-CFE) with different thickness.
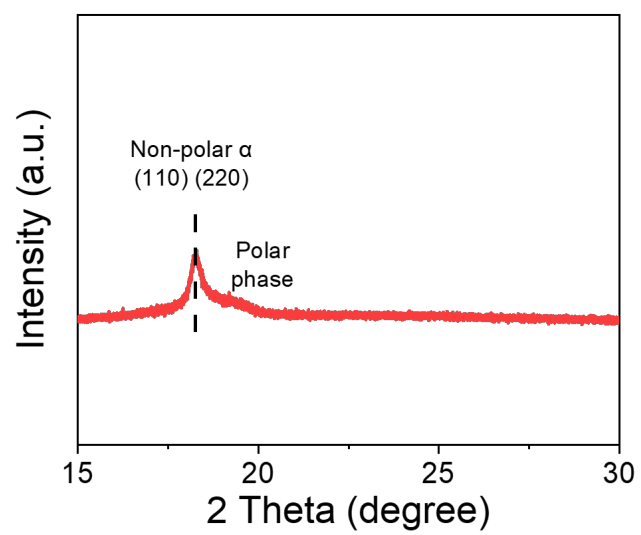
Fig. S17 XRD result of P(VDF-TrFE-CFE) film.
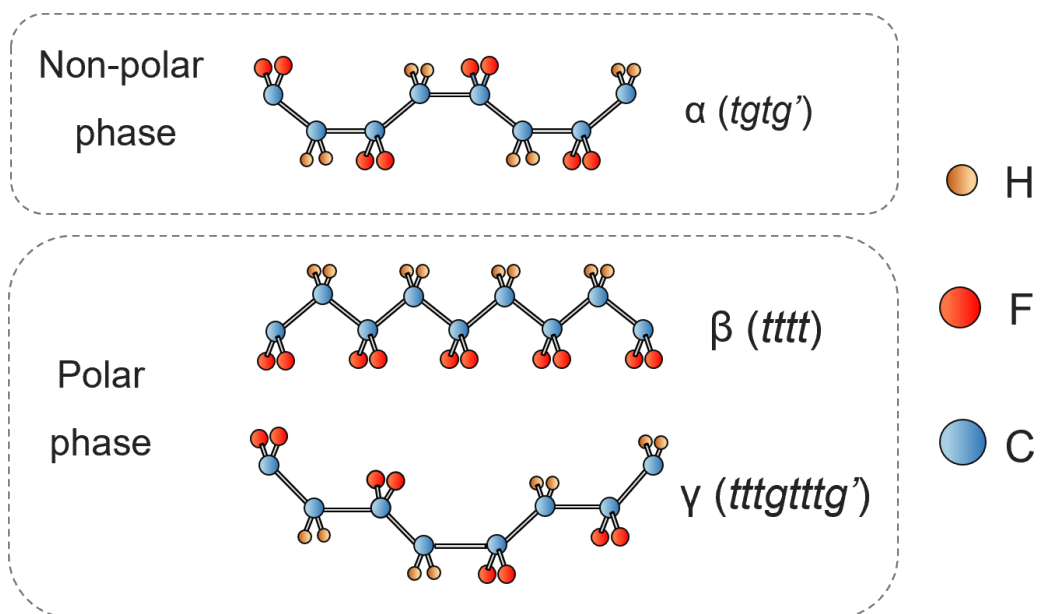
Fig. S18 Schematic chain conformations of P(VDF-TrFE-CFE).
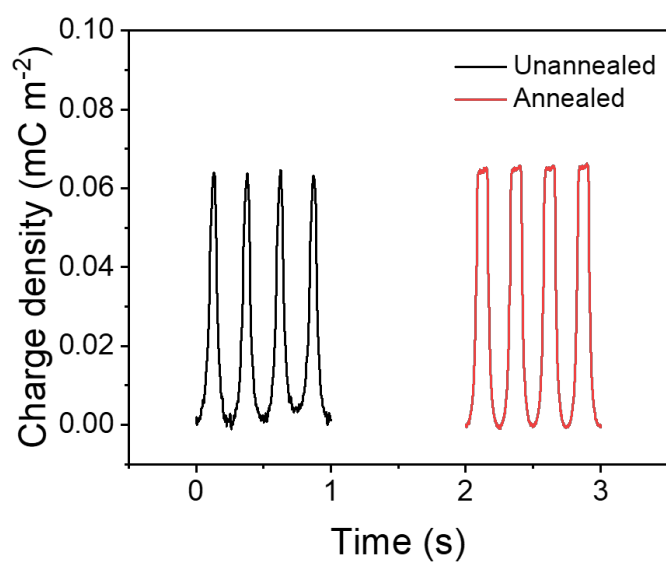
Fig. S19 Charge density of CS-TENG with unannealed and annealed P(VDF-TrFE-CFE) films (1.4 Hz).
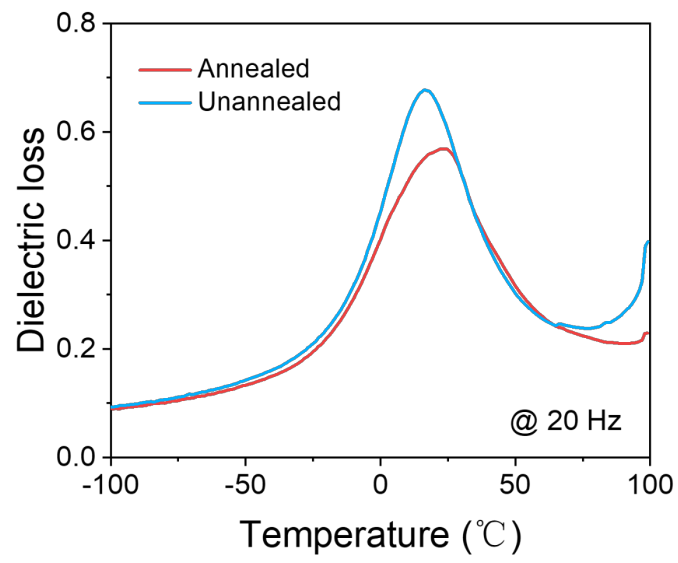
Fig. S20 Temperature-dependent dielectric loss of unannealed and annealed P(VDF-TrFE-CFE) films.
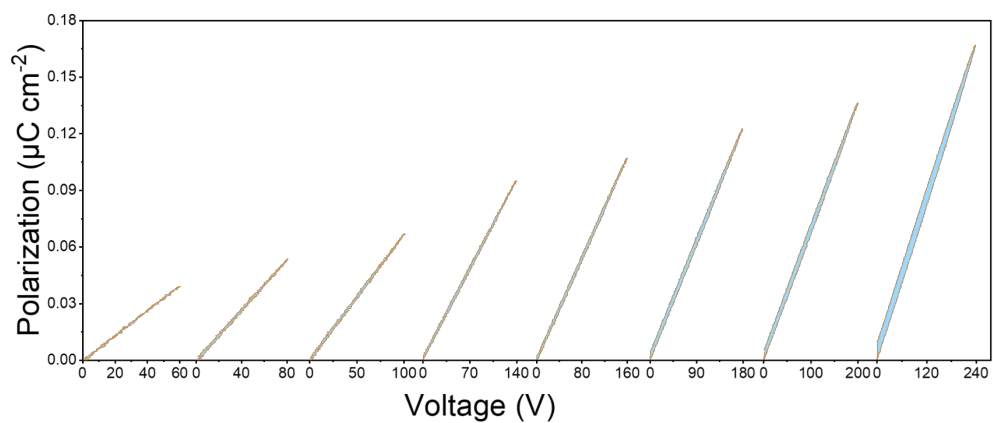
Fig. S21 The polarization loops of P(VDF-TrFE-CFE) film at different voltage.
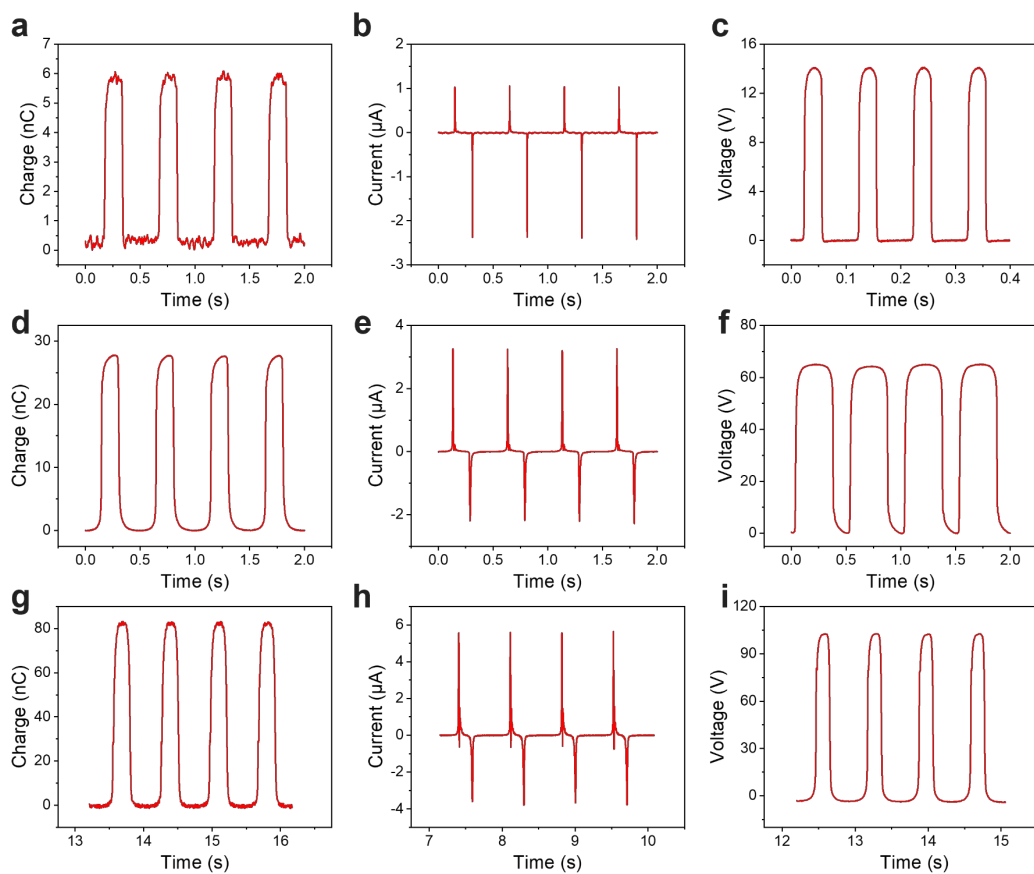
Fig. S22 The output performance of excitation TENG. (a) The charge, (b) current, (c) voltage of 1 cm^2 excitation TENG. (d) The charge, (e) current, (f) voltage of 4 cm^2 excitation TENG. (g) The charge, (h) current, (i) voltage of 10 cm^2 excitation TENG.
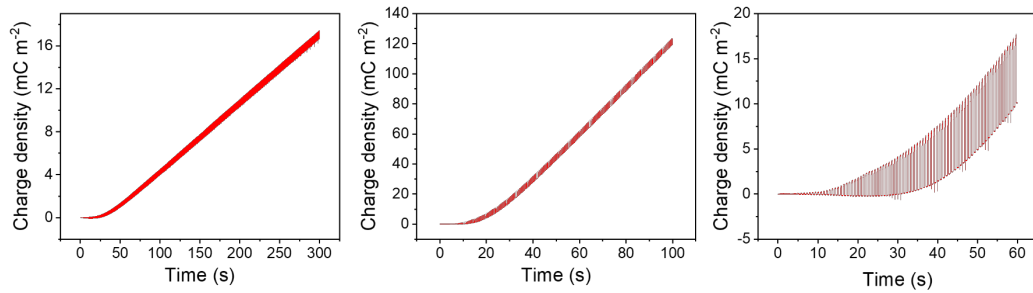
Fig. S23 The charge accumulation process of (a) ECE-TENG with 1 cm^2 external TENG and 1 cm^2 main TENG, (b) ECE-TENG with 4 cm^2 external TENG and 1 cm^2 main TENG, (c) ECE-TENG with 10 cm^2 external TENG and 1 cm^2 main TENG at 2 Hz.
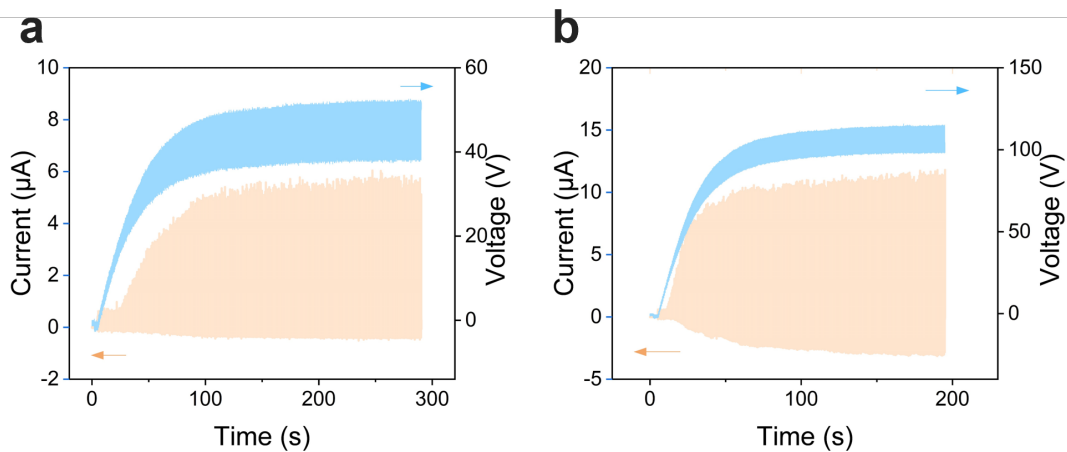
Fig. S24 The current and synchronous voltage of (a) ECE-TENG with 1 cm^2 external TENG and 1 cm^2 main TENG, (b) ECE-TENG with 4 cm^2 external TENG and 1 cm^2 main TENG at 2 Hz.
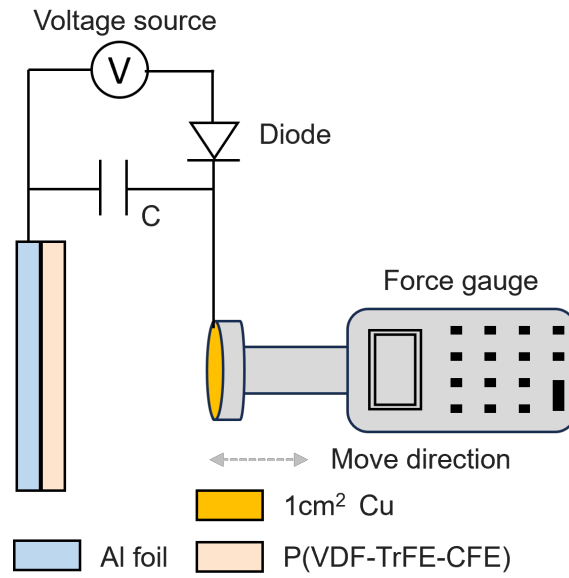
Fig. S25 The schematic diagram of the tensile force test (Voltage source: 300 V).
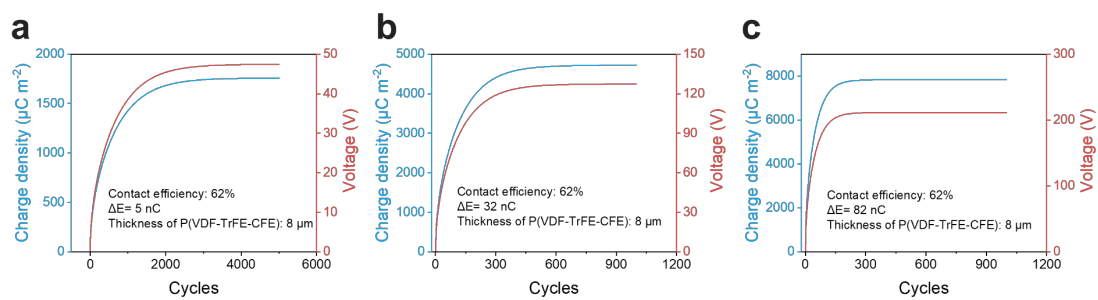
Fig. S26 The simulation curves of charge density and voltage for (a) ECE-TENG with 1 cm^2 external TENG and 1 cm^2 main TENG, (b) ECE-TENG with 4 cm^2 external TENG and 1 cm^2 main TENG, (c) ECE-TENG with 10 cm^2 external TENG and 1 cm^2 main TENG.
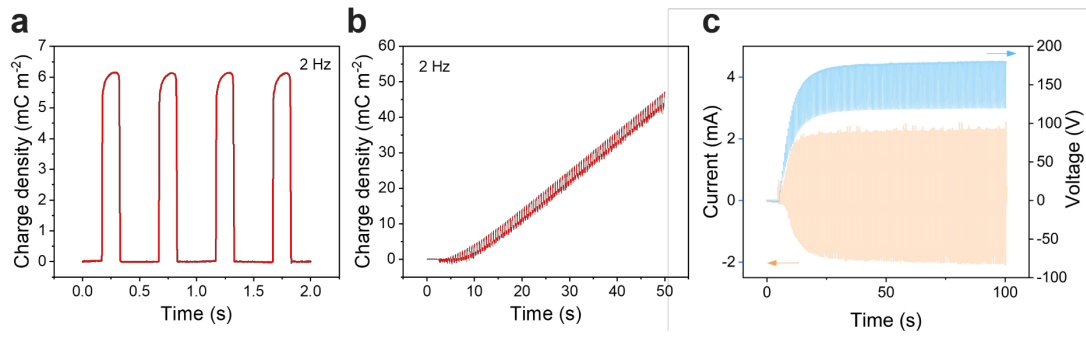
Fig. S27 (a) Charge density, (b) charge accumulation process, (c) current and synchronous voltage of ECE-TENG with 10 cm^2 external TENG and 4 cm^2 main TENG at 2 Hz.
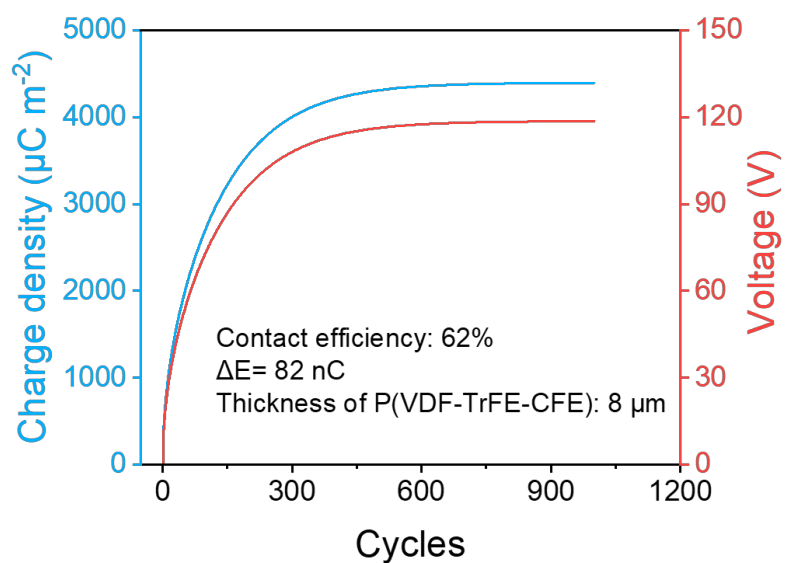
Fig. S28 The simulation curves of charge density and voltage for ECE-TENG with 10 cm^2 external TENG and 4 cm^2 main TENG
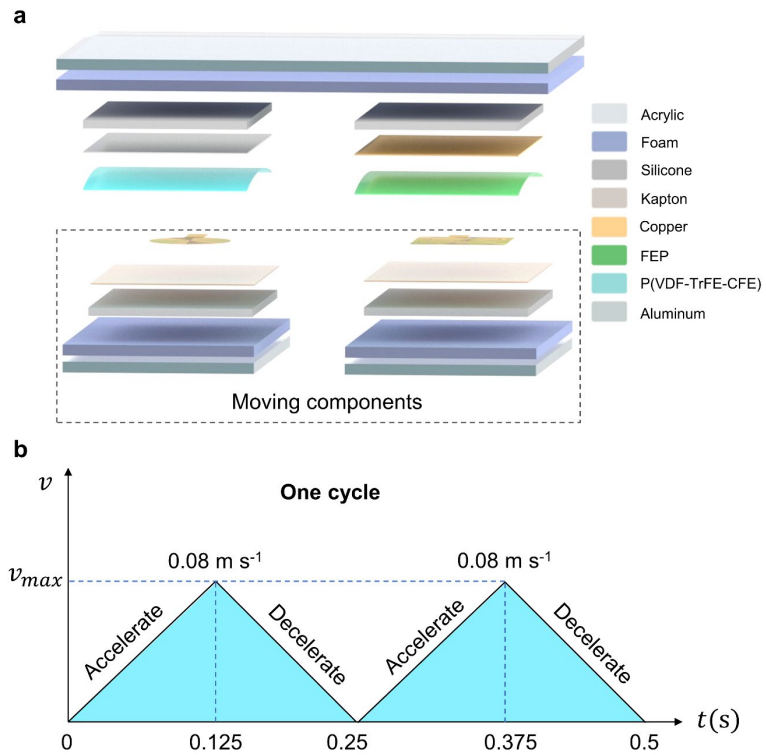
Fig. S29 (a) Schematically diagram of ECE-TENG. (b) The absolute value of instantaneous speed for moving components for ECE-TENG during one cycle.
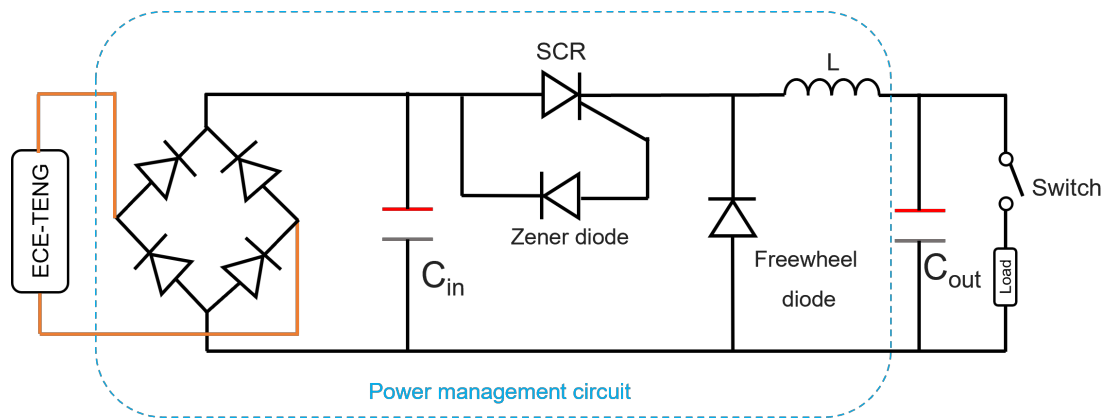
Fig. S30 Circuit diagram of the ECE-TENG with a power management circuit for powering energy storage and electronic equipment.
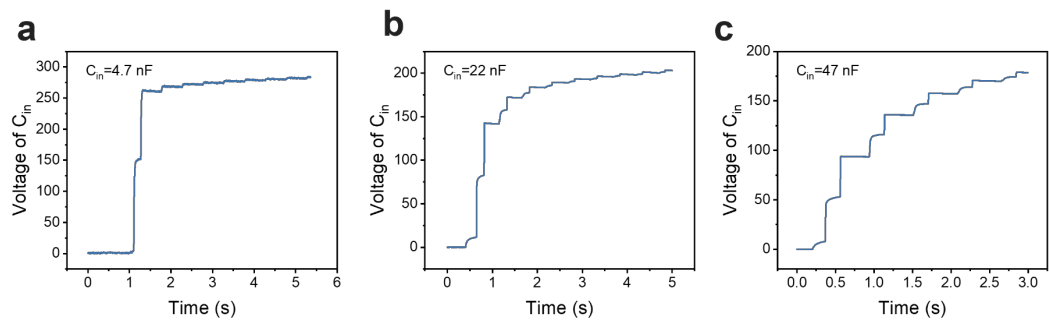
Fig. S31 Response of V_{Cin} to one cycle of ECE-TENG charge under different C_{in}. (a) 4.7 nF. (b) 22 nF. (c) 47 nF.
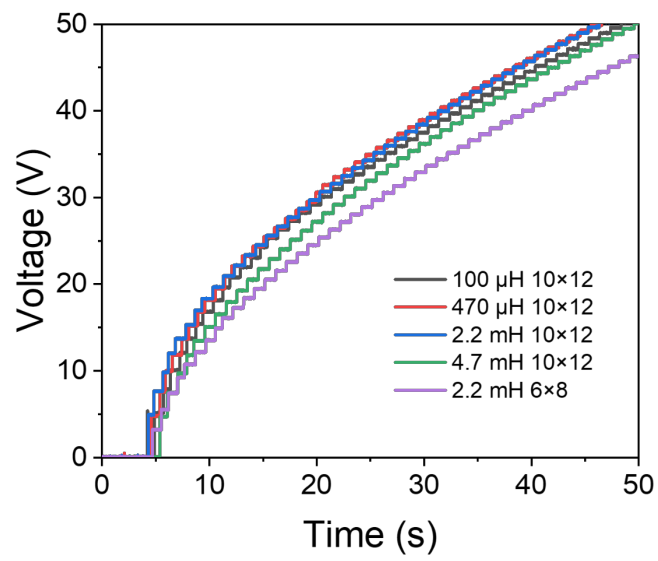
Fig. S32 Output voltage curves with different inductors (10×12 indicates that the magnetic core has a diameter of 10 mm and a height of 12 mm.).
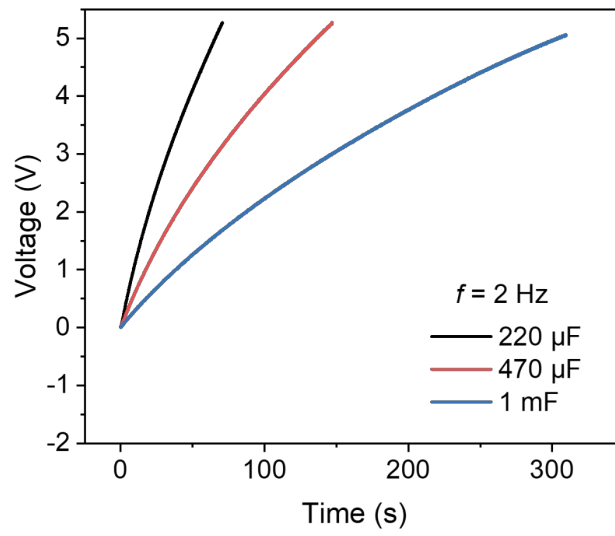
Fig. S33 Charging curves of different C_{out} for ECE-TENG without PMC.
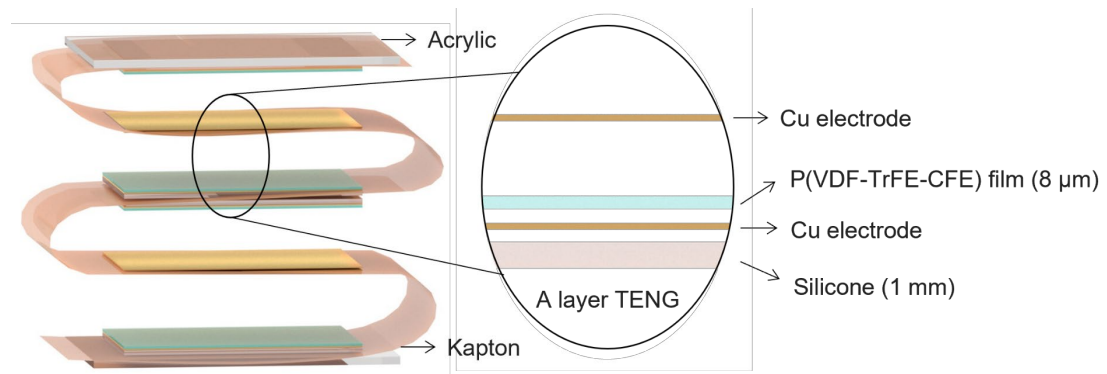
Fig. S34 Schematic diagram of multilayered TENG.

Supplementary Note 1: The detailed process of air breakdown in a TENG.

Specifically, primary electrons generated naturally near dielectric, are accelerated in the electric field and collide with gas molecules. Bound electrons are removed from the gas molecules by impact ionization and positively charged ions are formed. The ejected electrons are again accelerated by the external electric field and ionize further gas molecules. By repetition of these processes the number of electrons increases exponentially. Finally, electrons migrate upward and neutralize the positive charges in the upper electrode, and the positive ions move downward and deposit on the dielectric film surface, showing electric spark or arc phenomenon. Therefore, the air breakdown could limit the improvement of charge density and even make TENGs fail[1,2].

Supplementary Note 2: The detailed theoretical analysis process on achieving high charge density.

Specifically, the voltage forms between the top electrode and dielectric surface under a certain air gap (V_{gap}) for a CS-TENG. Based on parallel-plate model, the voltage at short-circuit condition can be derived and expressed by[3]:

$$V_{gap} = \frac{\sigma dx}{\varepsilon_0(d+\varepsilon_r x)} \tag{1}$$

Where σ is the triboelectric surface charge density on the electrode as a result of contact electrification. d and ε_r is the thickness and relative permittivity of the dielectric, respectively. ε_0 and x represent the vacuum permittivity ($\varepsilon_0 = 8.85 \times 10^{-12}$ F m⁻¹) and the distance between top electrode and dielectric.

In addition, according to Paschen's law[4], the breakdown voltage between two parallel plates can be determined empirically by

$$V_b = \frac{APx}{\ln(Px)+B} \tag{2}$$

Where P is the barometric pressure. x is the gap distance between two plates. A and B are the constants determined by atmosphere, including atmospheric composition, relative humidity, temperature, etc. A is inversely proportional to the relative humidity and proportional to maximum charge density. For a common ambient condition, $A = 2.87 \times 10^7$ $V\ atm^{-1}m^{-1}$, and $B = 12.6$.

Avoiding air breakdown requires V_b is always larger than V_{gap}. In this case, the maximum charge density for different dielectrics and ambient conditions can be deduced as:

$$\sigma_{max} = \left(\frac{AP\left(\varepsilon_0 + \frac{\varepsilon_0\varepsilon_r}{d}x\right)}{(\ln(Px)+B)}\right)_{min} \tag{3}$$

Supplementary Note 3: The principle of contact-separation TENGs.

For a contact-separation TENG in Fig. S5, Cu and P(VDF-TrFE-CFE) gradually come into contact under external force. Due to the triboelectric effect, when Cu and P(VDF-TrFE-CFE) are contact in physical, equal amounts of different triboelectric charges will be generated. Since P(VDF-TrFE-CFE) is an insulating polymer the triboelectric charges on the surface of P(VDF-TrFE-CFE) will be retained for a period of time. Next, when copper and P(VDF-TrFE-CFE) are gradually separated, due to the electrostatic induction effect, electrons will move from the Al foil to the Cu electrode in the external circuit until the maximum separation distance, thus generating a current flowing from Cu electrode to Al foil in the external circuit. Then when Cu and P(VDF-TrFE-CFE) come into contact again, due to electrostatic induction effect, electrons flow from Cu electrode to Al foil through the external circuit until complete contact, thus generating a current moving from Al foil to Cu electrode in the external circuit. Therefore, the AC signal is generated in the external circuit during contact-separation process.

Supplementary Note 4: The process of electrical breakdown for P(VDF-TrFE-CFE) film.

Electrons in P(VDF-TrFE-CFE) film are accelerated by the electric field and gain therefore kinetic energy. Electrons that gain sufficient energy will cause ionization during impact and generate more free electrons. If the process of impact ionization goes on, then the P(VDF-TrFE-CFE) will undergo breakdown due to an increased amount of highly energetic and mobile electrons.

Supplementary Note 5: The breakdown strength of P(VDF-TrFE-CFE).

Weibull statistics is utilized to analyze the experimental data of dielectric breakdown strength of P(VDF-TrFE-CFE). The characteristic breakdown strength is determined by fitting the data to a two-parameter Weibull distribution equation $P(E) = 1 - \exp\left[-(E_i/E_b)^\beta\right]$, where $P(E)$ represents the cumulative probability of electric failure, E_i is the experimental breakdown data, E_b is scale parameter referring to breakdown strength at the cumulative failure probability of 63.2% and is also regarded as the characteristic breakdown strength, and β shape parameter is the Weibull modulus associated with the dispersion of E_i.[5]

Supplementary Note 6: The distribution of voltage during separation.
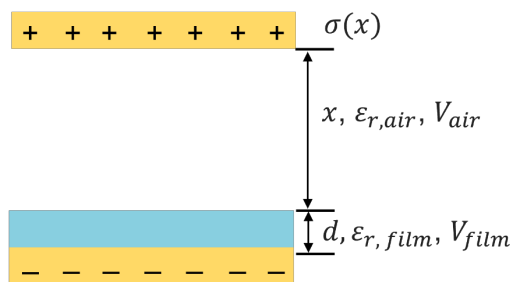
The voltage applied on film (V_{film}) and air (V_{air}) is determined by equation (5) and (6), respectively.

$$V_{film} = \frac{\sigma(x)}{C_{film}} = \frac{\sigma(x)d}{\varepsilon_0 \varepsilon_{r,film} S} \tag{4}$$

$$V_{air} = \frac{\sigma(x)}{C_{air}} = \frac{\sigma(x)x}{\varepsilon_0 \varepsilon_{r,air} S} \tag{5}$$

Where $\sigma(x)$ is charge amount at x separation distance. d, C_{film} and $\varepsilon_{r,film}$ are thickness, capacitance and dielectric permittivity of film. C_{air} and $\varepsilon_{r,air}$ are capacitance and dielectric permittivity of air. S is effective area of electrode. Thus, the ratio between V_{film} and V_{air} can be given:

$$\frac{V_{film}}{V_{air}} = \frac{\varepsilon_{r,air} d}{\varepsilon_{r,film} x} \tag{6}$$

For triboelectric layer, P(VDF-TrFE-CFE), it's dielectric permittivity and thickness are about 50 (1 kHz) and 8 μm, respectively. The maximum of separation distance x is 1 cm. Thus, the voltage across on P(VDF-TrFE-CFE) film approaches 0 V during separation.

Supplementary Note 7: The tensile force at high charge density during separation process.

We tested the tensile force during separation using force gauge and schematic diagram of test is shown in Fig. S25. The average tensile force is about 1.07 N for an ECE-TENG with 1 cm^2 effective area between P(VDF-TrFE-CFE) film and Cu electrode (The detailed results is shown in Supplementary Table 2), suggesting that very little work is required to separate them. Our all experiments in this work were tested on linear motor, so there is no need to consider the separation problem at greater contact area.

Supplementary Note 8: The negative effect of energy loss process on output performance.

To demonstrate the negative effect of energy loss process on output performance, we maintained a uniform charge accumulation process using the same external TENG of 10 cm^2. Simultaneously, we increased the energy loss process by enlarging the main TENG's area from 1 cm² to 4 cm². The increase in the area of P(VDF-TrFE-CFE) film typically leads to an improvement in the leakage current per unit area. This is because the probability of charge carriers encountering defects or impurities within the film increases as the area increases, resulting in a higher leakage current. Moreover, to exclude the influence of the contact efficiency of the main TENG, we ensured that the two main TENGs have the same contact efficiency by adjusting the motor. Corresponding calculation methods and results are shown in Supplementary Note 9 and Supplementary Table 1. Consequently, the increase of the energy loss process leads to a reduction in charge density from 8.6 mC m^{-2} to 4.4 mC m^{-2} (Fig. S27). Likewise, the experimental result and the simulation result of charge density and voltage are also approximately consistent (Fig. S28). These results demonstrate the negative effect of energy loss process and indicates a larger accumulation process is needed to reach the same equilibrium state with ECE-TENG of 1 cm^2.

Supplementary Note 9: The calculation of contact efficiency.

Here, the contact efficiency can be obtained with the following equation:

$$\eta = \frac{C_{contact}}{C_{film}} \tag{7}$$

Where $C_{contact}$ is the capacitance when main TENG getting compressed, and C_{film} stands for the capacitance of dielectric film with deposited electrodes.[6]

Supplementary Note 10: The discussion about conversion efficiency of mechanical energy into electrical energy for TENGs.

Generally, the conversion efficiency ($\eta_{M,E}$) of mechanical energy into electrical energy can be expressed as:

$$\eta_{M,E} = \frac{\overline{E_{out}}}{\overline{E_{in}}} \tag{8}$$

where $\overline{E_{out}}$ is the average output energy, and $\overline{E_{in}}$ is the average input energy.

As for $\overline{E_{out}}$, it can be easily measured through testing the current on a series of loads with different resistances to get the maximum electrical energy. For an ECE-TENG in this work, the maximum energy density is up to 0.808 J m^{-2} cycle^{-1} (shown in Fig. 5i in the manuscript). So, the $\overline{E_{out}}$ is about 8.08×10^{-5} J per cycle for a device with area of 1 cm^2.

However, accurately calculating the average input energy ($\overline{E_{in}}$) for the TENG presents challenges. Here are several methods to calculate conversion efficiency:

(1) The first method: using the motor's output as the input energy of the TENG. But due to the motor's design, the motor drives many non-TENG components, such as guide rods, sliding rods, etc., making it challenging to isolate the energy directed specifically towards the TENG.

(2) The second method: calculating the output energy to the TENG through the work done by force. The conversion efficiency of TENG is given by[7]:

$$\eta_{M,E} = \frac{\oint V dQ}{\oint F dx} \tag{9}$$

where V and Q are voltage drop and the charge transfer between two electrodes. F is the input force required to drive the TENG, x is the displacement. While the conversion efficiency of TENG in various modes can be determined using this approach, it is important to note that this method operates under ideal conditions. It assumes that all input force arises solely from the electrostatic force, neglecting the impacts of elastic force, friction force, air resistance, and other forces. Additionally, it assumes a fixed charge density on the surface, whereas, in reality, the charge density dynamically changes with cyclic contact separation. Therefore, this method also faces challenges in accurately calculating the input energy to the TENG.

(3) The third method: calculating the input energy by the kinetic energy of the TENG. The $\overline{E_{in}}$ of a TENG provided by motor is determined by (one cycle):

$$\overline{E_{in}} = 2 \times \int_{t=0\ s}^{t=0.25\ s} \frac{1}{2}mv^2(t)\,dt \tag{10}$$

where m, $v(t)$ and t are the mass, the absolute value of instantaneous speed and moving times of the TENG, respectively. The detailed schematically diagram of ECE-TENG in this work is shown in Fig. S29a, and the quality of moving components is about 18 g. Furthermore, for $v(t)$ of moving components, the separation distance and working frequency are set to 1 cm and 2 Hz, respectively. And during contact or separation process, the TENG is moving with uniform acceleration and uniform deceleration (0.64 m s^{-2}). Thus, the absolute value of instantaneous speed for moving components in one cycle can be obtained, as shown in Fig. S29b. According to the above parameters, the calculated $\overline{E_{in}}$ provided by motor is about 2.304×10^{-4} J per cycle.

Therefore, the $\eta_{M,E}$ is about 35%. According to the above analysis, further optimization of the mass and separation distance of the TENG is expected to yield an efficiency greater than that achieved under the aforementioned conditions. However, considering the following situation: when disregarding the mass of acrylic and foam (negligible buffer layer), the mass of the remaining moving components totals is about 2.53 g, and the calculated input energy amounts to approximately 3×10^{-5} J per cycle. As a result, the conversion efficiency obtained through this method exceeds 100%, primarily due to the neglect of electrostatic potential energy and elastic potential energy (which are challenging to calculate) when contact and separation are about to occur. Obviously, this approach also encounters challenges in accurately calculating the average input energy for the TENG.

(4) The fourth method: calculating the input energy using the design of spring. For instance, a sliding mode TENG was designed.[8] Springs were used to store mechanical energy and then converting stored mechanical energy in the spring into electrical energy. As for the input mechanical energy ($E_{mechanical}$), it was determined by the difference between potential energy at initial position (x = 1 mm) and final position (equilibrium

point), which was calculated by:

$$E_{mechanical} = E_{mechanical-x} - E_{mechanical-0} = 2kx^2 \tag{11}$$

where k is the spring constant of a single spring (k = 15.76 N m^{-1}), x is the displacement (x = 1 mm). As for output electrical energy ($E_{electrical}$), it was calculated through:

$$E_{electrical} = \int I^2 R dt \tag{12}$$

where I is the instantaneous current, R is the external resistance load. As a result, a high total conversion efficiency up to 85% can be achieved under the best matched resistance. However, it's worth noting that this method is computationally reasonable but is limited to sliding mode TENGs with spring designs.

It can be seen that the conversion efficiency is closely related to the structural design of TENG and there isn't a reasonable approach to accurately calculate the input energy for the contact-separation mode TENG utilized in this work.

Supplementary Note 11: Constant current in an RC circuit.

Time constant (τ) in an RC (Resistor Capacitor) circuit is:

$$\tau = RC \tag{13}$$

The voltage of C_{out} approaches zero only when the discharge time of C_{out} is approximately 5τ. Given that the motion period of the ECE-TENG is 0.5 s in this work, a constant current can be achieved when 5τ is much larger than 0.5 s.

Supplementary Note 12: Area assessment of ECE-TENG for charging a phone.

Our ECE-TENG exhibits an average energy density of 0.405 J m^{-2} cycle^{-1}, allowing it to deliver an average power of 2.025 W m^{-2} at 5 Hz. Charing a commercial phone demands a power of 5 W. Thus, an ECE-TENG with an effective area 2.5 m^2 can charge a phone.

When designing an ECE-TENG with an effective area of 2.5 m^2 in a multilayered structure as illustrated in Fig S34, each layer of the TENG is configured with an effective contact area of 25 cm². The Kapton layer has a thickness of 100 μm, and the thickness of the Cu electrode obtained by a magnetic method is on the order of nanometers, making it negligible. In theory, for a contact-separation mode TENG, when the separation distance is approximately 10 times the thickness of the triboelectric material, the transferred charge can reach 90% of the surface charge amount.[3] We set the separation distance to 2 mm based on practical experimental results.

According to the above design, the volume of a single layer of the TENG is approximately 8×10^{-6} m³. Consequently, our TENG, with an effective volume of 8×10^{-3} m³ in the separation state, can charge a phone.

Supplementary Table 1: The comparison of contact efficiency in two main TENGs.

Main TENG's area	1 cm²	4 cm²
$C_{contact}$	3.7 nF	14.8 nF
C_{film}	6 nF	24 nF
η	61.7%	61.7%

Test frequency of capacitance is 100 Hz.

Supplementary Table 2：The results of tensile force for ECE-TENG with P(VDF-TrFE-CFE).

	1st	2nd	3rd	4th	5th	Average
Tensile force (N)	1.04	1.06	1.06	1.08	1.1	1.07

Video 1 Hygrothermographs powered by ECE-TENG with P(VDF-TrFE-CFE)

Video 2 Commercial LED bulbs powered by ECE-TENG with P(VDF-TrFE-CFE)

References

1. J.S. Townsend, *Nature*, 1900, **62**, 340-341.
2. J.S. Townsend, *J. Franklin Inst.*, 1925, **200**, 563-590.
3. S. Niu, , S. Wang, L. Lin, Y. Liu, Y.S. Zhou, Y. Hu and Z.L. Wang, *Energy Environ. Sci.*, 2013, **6**, 3576-3583.
4. J. Wang, C. Wu, Y. Dai, Z. Zhao, A. Wang, T. Zhang and Z.L. Wang, *Nat. Commun.*, 2017, **8**, 88.
5. Z. Dai, Z. Bao, S. Ding, C. Liu, H. Sun, H. Wang, X. Zhou, Y. Wang, Y. Yin and X. Li, *Adv. Mater.*, 2022, **34**, 2101976.
6. Y. Liu, W. Liu, Z. Wang, W. He, Q. Tang, Y. Xi, X. Wang, H. Guo and C. Hu, *Nat. Commun.*, 2020, **11**, 1599.
7. G. Xu, X. Li, X. Xia, J. Fu, W. Ding and Y. Zi, *Nano Energy*, 2019, **59**, 154-161.
8. Y. Xie, S. Wang, S. Niu, L. Lin, Q. Jing, J. Yang, Z. Wu and Z. L. Wang, *Adv. Mater.*, 2014, **26**, 6599-6607.